Authigenic $^{10}Be/^{9}Be$ dating of the Horná Štubňa river terrace points to the inception of the terrace staircase formation to the next row Turiec Basin (Slovakia) from the Middle Pleistocene transition

Kishan Aherwar[1], Michal Šujan[1,2], Andrej Chyba[3], Barbara Rózsová[1] & Aster Team[4*]

[1] Department of Geology and Paleontology, Faculty of Natural Sciences, Comenius University in Bratislava, Ilkovičova 6, 842 15 Bratislava, Slovakia; aherwar1@uniba.sk
[2] Laboratory of Quaternary Research, State Research Institute Nature Research Centre, 2 Akademijos Str., LT-08412, Vilnius, Lithuania, michal.sujan@gamtc.lt
[3] Institute of Chemistry, Slovak Academy of Sciences, Dúbravská cesta 9, 845 38 Bratislava, Slovakia; Andrej.chyba@savba.sk
[4] CNRS-IRD-Collège de France-INRA, CEREGE, Aix-Marseille Univ., 13545 Aix-en-Provence, France; aumaitre@cerege.fr
* Georges Aumaître, Karim Keddadouche, Fawzi Zaidi

AGEOS

Abstract: Despite the extensive presence of river terraces in the Central Western Carpathians, geochronological proxies for their formation are scarce, particularly concerning Middle and Lower Pleistocene accumulations. This study employs authigenic $^{10}Be/^{9}Be$ dating on a Horná Štubňa river terrace outcrop in the southern Turiec Basin, with an expected age of > 500 ka, as the settings prohibit the use of other, more established methods. The dating focused on floodplain muds, situated above angular gravels deposited by the debris flow process and below rounded sandy gravel deposited by a debris flood. Five ages were obtained, showing a scattered distribution ranging from 724–394 ka, after excluding one outlier sample. However, correcting the dating, which involved considering the age and uncertainty of the initial $^{10}Be/^{9}Be$ ratio calibration site Veľký Čepčín, resulted in an age range of 690–1020 ka, with a mean weighted age of 838.0 ± 83.3 ka. These findings suggest that the climatic changes associated with the Middle Pleistocene transition may have influenced base-level changes in the Turiec Basin, as the studied terrace represents the second-highest level of the preserved staircase. The documented low incision rate of ~ 0.03–0.04 mm·a^{-1} deviates from an order of magnitude higher values determined from the Outer Western Carpathians but agrees with the values established for the Pannonian Basin, Transdanubian Range and Eastern Alps.
Key words: Western Carpathians, Quaternary, fluvial sediment, intramontane basin, cosmogenic nuclides

1. INTRODUCTION

River terraces serve as a vital archive for understanding terrain evolution, forming in response to base level and climate changes, apart from possible anthropogenic forcing (Starkel et al., 2007; Vandenberghe, 2008; Gibbard & Lewin, 2009; Necea et al., 2013; Olszak & Adamiec, 2016; Olszak, 2017; Tlapáková et al., 2021). Chronostratigraphic models of river terrace depositional archives enable precise reconstruction of uplift/incision histories in terrestrial environments (e.g., Starkel et al., 2007; Kováč et al., 2011; Viveen et al., 2012; Necea et al., 2013; Šujan & Rybár, 2014; Olszak & Adamiec, 2016; Novák et al., 2017; Olszak, 2017; Schumacher et al., 2018; Vitovič & Minár, 2018; Olszak et al., 2019; Olszak & Alexanderson, 2020; Ruszkiczay-Rüdiger et al., 2020; Tlapáková et al., 2021; Sládek et al., 2022; Šujan et al., 2023c). Consequently, fluvial terraces represent a prime focus for integrated geomorphological and geochronological investigations. However, some dating techniques, such as radiocarbon or luminescence dating, have limited applicability to narrow time ranges, prompting the utilization of new methods. Authigenic $^{10}Be/^{9}Be$ dating stands out as one such radiometric dating tool, thanks to its theoretical range of up to 14 Ma (e.g., Bourlès et al., 1989; Lebatard et al., 2008; Šujan et al., 2016).

The current state of knowledge of incision rates based on river terrace depositional archives in the Western Carpathians (WC) mostly originates from its northern periphery, from the terrace systems formed above the Paleogene nappes of the Outer WC flysch zone. The specific rates determined here range from ~ 0.15–0.30 mm·a^{-1} (Starkel et al., 2007), ~ 0.5 mm·a^{-1} (Olszak & Alexanderson, 2020), ~ 0.6 mm·a^{-1} (Olszak & Adamiec, 2016) and ~ 0.25–1.10 mm·a^{-1} Olszak et al. (2019). The Žiar Basin in the Central WC experienced an incision rate of < 0.12 mm·a^{-1}, based on a single OSL age of Sládek et al. (2022). A much more pronounced base-level fall of ~ 0.8–1.0 mm·a^{-1} in the eastern Central WC was attributed to the offset of the Vikartovce fault (Vojtko et al., 2011). The western periphery of the WC exhibits relatively low incision rates of ~ 0.2 mm·a^{-1} (Novák et al., 2017; Tlapáková et al., 2021). When it comes to transitioning towards the Neogene basins southwards the WC, the incision rates are even lower, reaching < 0.08 mm·a^{-1} in the Vienna Basin (Braumann et al., 2019), ~ 0.04 mm·a^{-1} in the eastern Danube Basin (Šujan et al., 2023c), and long-term stable incision rates of ~ 0.05 mm·a^{-1} supported by the extensive river terrace archive of the Transdanubian Range (Ruszkiczay-Rüdiger et al., 2018, 2020). The Eastern Alps were subject to similar, low-intensity incision rates of ~ 0.06–0.2 mm·a^{-1} during the last few million years (Wagner et al., 2010, 2011; Legrain et al., 2014; Häuselmann et

Manuscript received 2024-04-30
Revised version accepted 2024-06-17

al., 2020). On the other hand, the Southern Carpathians exhibit incision rates in the order of ~ 0.5–1.0 mm·a^{-1} (Necea et al., 2005, 2013), similar to the Outer WC and in contrast to the internal zones of the WC mountain range. To sum up, there is a clear blind spot between the well-established incision rate models from the Outer WC and the Pannonian Basin System on the south, or towards the western WC periphery.

This study presents a series of authigenic ^{10}Be/^{9}Be ages obtained from a terrace located near the village of Horná Štubňa in the southern part of the Turiec Basin, which is bordered by the mountain horsts of the WC (Slovakia) (Kováč et al., 2011; Sládek et al., 2022). The dating aims to contribute to the issue of river terrace chronostratigraphy and incision rate determination, which is poorly investigated in the Central WC. The river terrace base is situated approximately 24–30 m above the local erosional base, represented by the channels of the present-day river network. Assuming an age range of ~ 370–220 ka of the Veľký Čepčín site (Holec & Braucher, 2014), situated just 6 meters above the Turiec River (the primary stream in the basin catchment), the anticipated age of the Horná Štubňa terrace exceeds 500 ka, as estimated by Kováč et al. (2011). This context underscores the preference for cosmogenic nuclide dating methods to date the river terrace fluvial deposit (Dunai, 2010), thus motivating the objective of the present study to date the fluvial terrace sediments.

2. GEOLOGICAL SETTINGS

The Western Carpathian orogen, situated within the Alpine-Carpathian mountain chain (Fig. 1A,B), attained its present configuration during the Cretaceous-Miocene Alpine orogenesis. This was a complex and protracted process, propelled by the subduction of oceanic crust beneath the advancing orogenic wedge and the northeastward escape of the Alpine-Carpathian-Pannonian microplate toward an embayment of the North European Platform. The paleo-Alpine orogeny resulted in the stacking of thick-skinned nappe of the Tatric Unit, comprising crystalline basement and its late Paleozoic and Mesozoic cover sequences, along with the overlying thin skinned Fatric and Hronic nappes primarily composed of Mesozoic carbonate rocks. These units, along with remnants of the Central Carpathian Paleogene Basin, primarily located beneath the basin fill, form the basement and encircling mountains of the Turiec Basin (Hók et al., 2014; Králiková et al., 2014; Kováč et al., 2016; Plašienka, 2018).

The major subsidence of the Turiec Basin commenced in the Middle Miocene (Hók et al., 1998; Kováč et al., 2011), characterized by significant volcanic activity along its southern margin originating from the Kremnické vrchy Mts. (Fig. 1C), which are part of the Central Slovakia Volcanic Field (Konečný et al., 1995; Lexa et al., 2010). During the Late Miocene, the basin accumulated sediments reaching up to 1250 m (Fig. 1C), largely attributed to the presence of Lake Turiec and its regression ca. 7 Ma (Kováč et al., 2011; Pipík et al., 2012; Šujan et al., 2023b). The disappearance of the lake resulted from the onset of uplift in the surrounding mountain horsts, eventually establishing the current morphotectonic framework. This phase of uplift is anticipated to disrupt the planation surface (Šujan et al., 2023b), previously formed during a period of relative tectonic stability (Minár et al., 2011), and led to the distinct basin-and-range structure observed in the Western Carpathians (Nemčok & Lexa, 1990; Kováč & Hók, 1993).

Some base-level oscillations are discernible through the presence of the Pliocene Bystrička Formation and the Pleistocene Podstráne and Diviaky Formations, all originating from alluvial and alluvial fan processes (italics Blikra & Nemec, 1998; Plink-Björklund, 2021). However, accommodation rates diminished following the disappearance of Lake Turiec. A general decline in base level, driven by neotectonic dome-like uplift, resulted in the partial denudation of Miocene deposits and erosional contact with younger strata (Kováč et al., 2011; Minár et al., 2011). A more comprehensive understanding of the Pleistocene evolution of the basin is impeded by a lack of radiometric dating of Pleistocene sediments, with the Veľký Čepčín alluvial fan accumulation, dated to ~ 370–220 ka, serving as the sole tie-point (Holec & Braucher, 2014).

The Horná Štubňa river terrace, the focus of this study, is located in the southeastern part of the Turiec Basin (Fig. 1D). Its age was previously estimated to be ~ 500 ka, primarily based on its geomorphological position as the highest level of the local terrace staircase (Kováč et al., 2011). The terrace is exposed in a small quarry near a landfill (Fig. 2), occasionally excavated for sandy and gravelly material, which likely served for local construction purposes. The landfill is present within a gully, which enters a narrow floodplain of the Mútnik stream (Fig. 2). The base of the terrace, represented by the erosional surface underlying the river terrace accumulation, lies at an elevation of 559.5 m a.s.l. and reaches a height of ~ 4 m. The nearest section of the Turiec River channel (in terms of aerial distance), the major stream draining the basin, is located at an elevation of 529.5 m a.s.l., while its tributary (Mútnik), located near the outcrop (Fig. 2), has a channel at an elevation of 535.5 m a.s.l. Hence, the erosional base of the Horná Štubňa river terrace appears 24–30 m above the present-day river network erosional base.

3. METHODS

3.1. Field research and stratigraphy

The investigated outcrop is situated within an intermittently excavated small quarry, featuring approximately a ~ 4.5-meter high subvertical outcrop wall. Documentation of the outcrop involved standard facies analysis and vertical profile logging (Stow, 2005). The broader stratigraphic context of the area was examined through lithological logs obtained from boreholes archived in the Geofond digital repository of the State Geological Institute of Dionýz Štúr in Bratislava, Slovakia. The logs were compiled in a generalized stratigraphic section. Specifically, the well profile HV-1 can be found in the report by Tužinský et al. (1967), GHŠ-1 is documented in Gašparik (1972), MS-1, MS-2, and MS-3 were conducted by Šujan & Dzúrik (1996) and the borehole profiles of V-5 and V-6 are included in Šustek (2001). All mentioned reports are available online at https://da.geology.

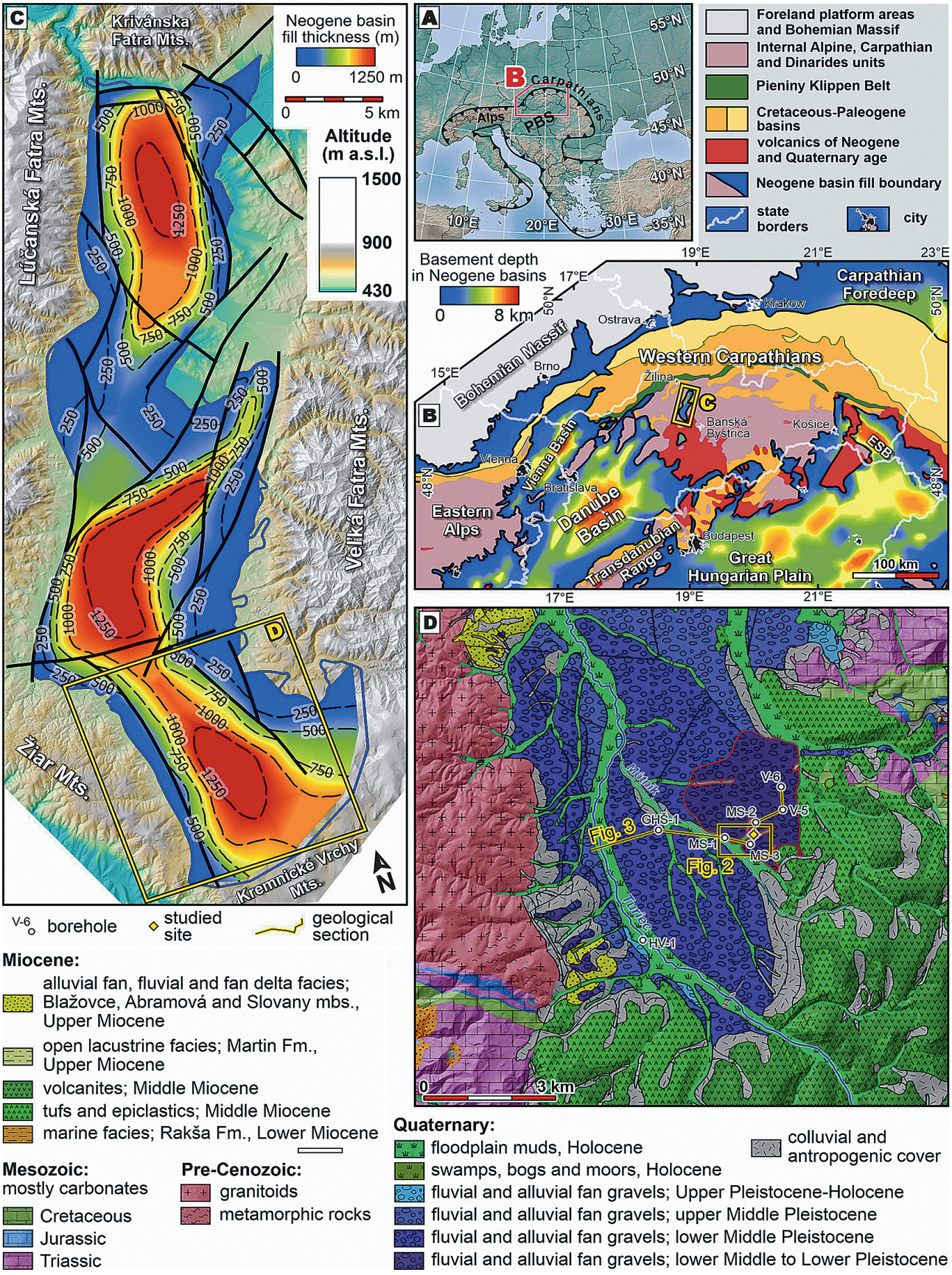

Fig. 1. Location of the Carpathian-Pannonian region in Europe (A) and the Turiec Basin in the Western Carpathian orogen (B). (C) Thickness of the Miocene to Quaternary successions of the Turiec Basin. (D) Geological map of the surroundings of the Horná Štubňa river terrace, analyzed in this study (modified from Gašparik & Halouzka, 1993). (A), (B) and (C) are modified from Šujan et al. (2024).

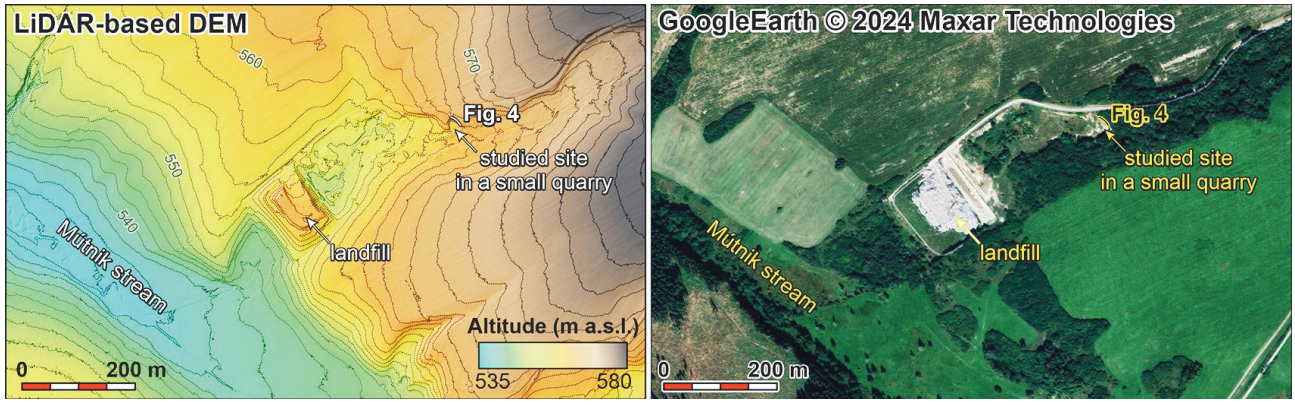

Fig. 2. Location of the studied site using LiDAR-based digital elevation model and aerial photograph obtained using Google Earth Pro software (version 7.3.6.9796). The contours in the digital elevation model map are spaced by 2 m. The Lidar DEM data were provided by the Geodesy, Cartography and Cadaster Authority of the Slovak Republic (online at: https://zbgis.skgeodesy.sk/mkzbgis/en/) – location in Fig. 1D.

sk/navigator/?desktop=Public. Setting up an account is necessary for access.

3.2. Authigenic $^{10}Be/^{9}Be$ dating

The infrequent usage of the authigenic $^{10}Be/^{9}Be$ dating stems from its complexity, which arises from the distinct sources of the two isotopes. Radioactive ^{10}Be is generated in the atmosphere through the interaction of cosmic rays with oxygen and nitrogen, whereas ^{9}Be originates from the chemical weathering of rocks (Raisbeck et al., 1981; Measures & Edmond, 1983; Brown et al., 1992). Both isotopes become incorporated into the authigenic phase, primarily composed of iron and manganese oxyhydroxides that form around the surface of sediment particles dispersed in a water column (Bourlès et al., 1989; Willenbring & von Blanckenburg, 2010; Wittmann et al., 2012; Singleton et al., 2017). Consequently, when these two isotopes converge in a water column, their initial ratio becomes influenced by various factors such as the petrography of the source area, denudation rate, and precipitation intensity (Willenbring & von Blanckenburg, 2010). Furthermore, the isotopic ratio signature undergoes alteration due to penecontemporaneous and post-depositional processes, including pedogenesis and the diagenetic release of beryllium into pore waters, upon sediment particle deposition (Dixon et al., 2018; Deng et al., 2023).

Hence, a robust determination of the initial $^{10}Be/^{9}Be$ ratio is a prerequisite for the effective application of the dating method, which employs the radioactive decay of ^{10}Be with a half-life of 1.387 ± 0.02 Ma (Chmeleff et al., 2010; Korschinek et al., 2010). By establishing the initial ratio R_0, the radiometric depositional age could be calculated using the equation $R = R_0 \times e^{-\lambda t}$, where R is the measured isotopic $^{10}Be/^{9}Be$ in the sample, λ the decay constant of ^{10}Be and t the time elapsed since deposition, can be used to determine the age of the deposited sediment. However, it is suggested to determine carefully the initial authigenic ratio R_0. A complex investigation of the initial $^{10}Be/^{9}Be$ ratio in the Turiec Basin was performed by Šujan et al. (2023b), assuming geochemical and mineralogical proxies of paleoenvironmental conditions, resulting in the use of the value 143.36 ± 1.41 ($\times 10^{-11}$) determined at the Veľký Čepčín outcrop for authigenic $^{10}Be/^{9}Be$ age calculation of terrestrial deposits. This ratio was employed in the present study. However, considering the age of the Veľký Čepčín succession reaching ~ 370–220 ka (Holec & Braucher, 2014), the obtained ages should be corrected with the addition of 295 ka (median of the range) and a further uncertainty of 75 ka included in the analytical uncertainty.

Six samples were taken from a floodplain muddy horizon, which appears between two gravelly units exposed in the Horná Štubňa river terrace outcrop. The sample preparation methodology used in this study is described in detail by Šujan et al. (2023a). Sample processing for both, accelerator mass spectrometry (AMS) and inductively coupled plasma-mass-spectrometry (ICP-MS) measurement was carried out at the Department of Geology and Paleontology Laboratory, Faculty of Natural Sciences, Comenius University Bratislava. The methodology for authigenic phase extraction is based on Bourlès et al. (1989). An amount of ~ 2.25 g crushed and dried sample was leached in a solution of 0.04 M NH_2OH–HCl in 25% acetic acid for 7 hours at ~ 95°C to extract the authigenic phase. ICP-MS measurement of 9Be was performed on aliquots of ~ 2 ml taken from the leaching solution, employing linear regression to mitigate the matrix effect (Tan & Horlick, 1987).

LGC ICP-MS beryllium standard solution in the amount of ~ 450 µl was added to the main fraction of the solution, having a $^{10}Be/^{9}Be$ ratio in the range of 3.42×10^{-15} to 3.61×10^{-15} concentration 1000 ppm. The spiked solution underwent evaporation and purification through column chromatography to isolate beryllium from other elements (Merchel & Herpers, 1999). The samples were oxidized and the obtained BeO powder mixed with Niobium powder was filled into copper cathodes for AMS measurements.

The ICP-MS measurements were performed using PlasmaQuant ICP-MS System (Analytik Jena AG) at the Institute of Chemistry, Slovak Academy of Sciences. Isotopic $^{10}Be/^{9}Be$ ratio measurement was performed at French National AMS facility ASTER, CEREGE Aix-en-Provence (France). The measurements were calibrated directly against the STD11 in-house standard ($^{10}Be/^{9}Be$ value of 1.191 ± 0.013 ($\times 10^{-11}$)) (Braucher et al., 2015). Analytical uncertainties (reported as 1σ) include uncertainties associated with AMS counting statistics, two

chemical blanks measurements and the AMS internal error (0.5%). Calculated ages include also the uncertainty associated with the initial ratio.

3.3 Fe, Mn, and Al analysis in the authigenic phase

The leaching solution employed during sample processing primarily targets the authigenic phase of elements adhered to the sediment surface. This phase mainly consists of iron and manganese oxyhydroxides and is recognized as the principal carrier of beryllium isotopes (Wittmann et al., 2012). Additionally, the concentrations of iron, manganese, and aluminum were determined in the aliquots extracted for beryllium-9 concentration analysis via ICP-MS. The concentrations are reported in ppm normalized to the total leaching solution volume.

4. RESULTS

4.1. Stratigraphy based on borehole profiles

The geological section across the studied site, oriented generally in a west-east direction and based on seven archival borehole lithological logs and the geological map, is shown in Fig. 3. The terrain gently rises from the Turiec River floodplain towards the east. It reaches an area covered by river terraces according to the geological map (0.4–2.5 km along the section), although borehole data confirming their presence are unavailable. The middle part of the section traverses two sections of the Mútnik Stream floodplain, where the accumulation of Holocene sediments is presumed. MS-1 well indicates the presence of a thin layer of gravel with mud, interpreted as a river terrace level. Further east, the section reaches the landfill near the studied outcrop in the 3.5–3.6 km interval of the section (Fig. 2). The section shows a river terrace in the range of 3.8–4.5 km, which has been documented by MS-2 well (muddy gravels) and by the outcrop investigated in this study. The uppermost part of the section reveals another river terrace at the highest elevation, ranging from 520 to 590 m a.s.l., as documented by V-5 and V-6 wells.

The majority of the shown Quaternary deposits are underlaid by the Miocene successions, which according to Gašparik & Halouzka (1993), Kováč et al. (2011) and Šujan et al. (2023b) should comprise the Upper Miocene Martin Fm., consisting of open lake muddy strata with sandy and gravelly intercalations. An exception could be seen in the highest point around the V-5 well, where the Quaternary base overlies Miocene volcanites (Fig. 3).

4.2. Facies on the outcrop

Description: The studied outcrop faces southwest. The exposed strata gently dip towards the northwest at approximately a 3° inclination (Fig. 4A). The lowermost part (4.73–4.05 m) consists of grey faintly laminated sandy mud (Fl facies) with an intercalation of well-rounded granules forming a clast-supported structure in a sub-horizontal layer ~ 10 cm thick (Ghk) (Fig. 4C, D). This interval is overlain by a layer of massive, matrix-supported gravel (~ 1.65 m thick) (Gmm, Fig. 4C), comprising chaotically arranged andesite and rhyolite clasts ranging from granules to boulders, predominantly angular with less sub-angular specimens (Fig. 5A). The matrix consists of light grey sandy mud. Above this layer, there is a horizon of distinctly horizontally laminated grey mud (Fhp), transitioning smoothly upwards to dark grey and black, spanning 2.05–2.30 m of the outcrop (Fig. 4B). This

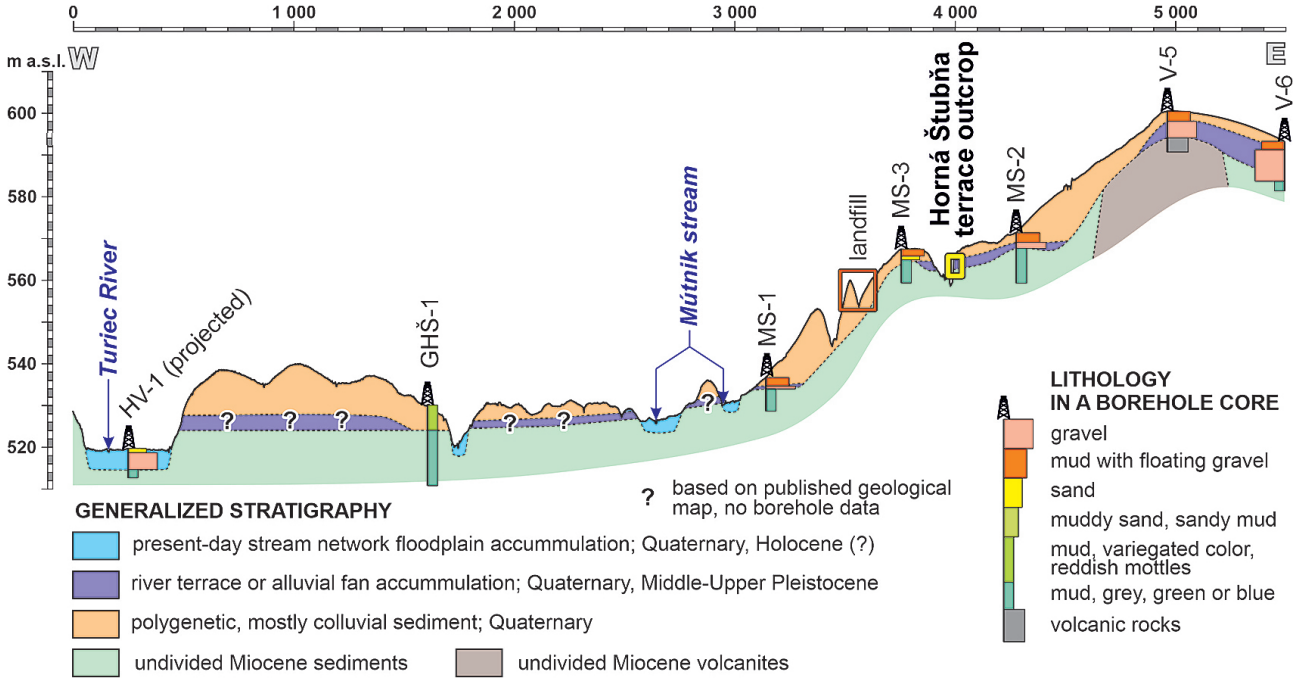

Fig. 3. Generalized stratigraphic section across the study area, based on archival boreholes and the geological map by Gašparik & Halouzka (1993) in the case of no borehole information. Location in Fig. 1D.

layer is covered by distinctly horizontally laminated reddish mud (1.60–2.05 m) and distinctly horizontally laminated beige mud with reddish intercalations (1.00–1.60 m), both categorized as Fhw facies (Fig. 4B). The uppermost unit comprises ~ 1 m thick massive matrix-supported gravel, primarily consisting of well-rounded pebbles and cobbles of andesites and rhyolites (Fig. 5B), embedded in reddish sandy matrix (Gmk) (Fig. 4B, D).

Depositional process interpretation: The facies Fl was deposited in subaquatic conditions by slow traction currents or hyperpycnal flows (Mulder et al., 2003; Yawar & Schieber, 2017), probably at the bottom of Lake Turiec, bearing a strong resemblance to the strata of the Martin Fm. (Šujan et al., 2023b). The gravelly intercalation of Ghk likely represents a gravity current deposit generated by a nearby deltaic feeder system (Talling et al., 2012). Alternatively, it might have been transported to the lake bottom by a storm current (Jelby et al., 2020). Moving upward, the ~ 1.65 m thick Gmm unit with angular granules to boulders exhibits characteristics typical of subaerial cohesive debris flow (Pierson & Costa, 1987; Brenna et al., 2020), suggesting a change in the depositional environment. The unit possibly consists of amalgamated products of several depositional events. Its base is interpreted as the erosional contact between Quaternary and Miocene successions. The overlying muddy horizon of Fhp facies suggests deposition from slowly flowing (0.2 $m \cdot s^{-1}$) or standing water column (Yawar & Schieber, 2017), with an increasing rate of organic matter accumulation upward, which remains undecomposed. This likely resulted from poorly drained floodplain conditions, associated with a high groundwater level and low oxygen availability (Aslan & Autin, 1999; Campo et al., 2016). Such settings were attained in a floodplain lake or an oxbow lake (Davies-Vollum & Kraus, 2001). Conditions changed upwards to a well-drained floodplain, as the laminated mud displays variegated colors with reddish markings indicating preserved oxidized iron in the strata (Aslan & Autin, 1999; Campo et al., 2016). The uppermost Gmk unit was probably deposited by distinct abrupt events of debris flood rather than by

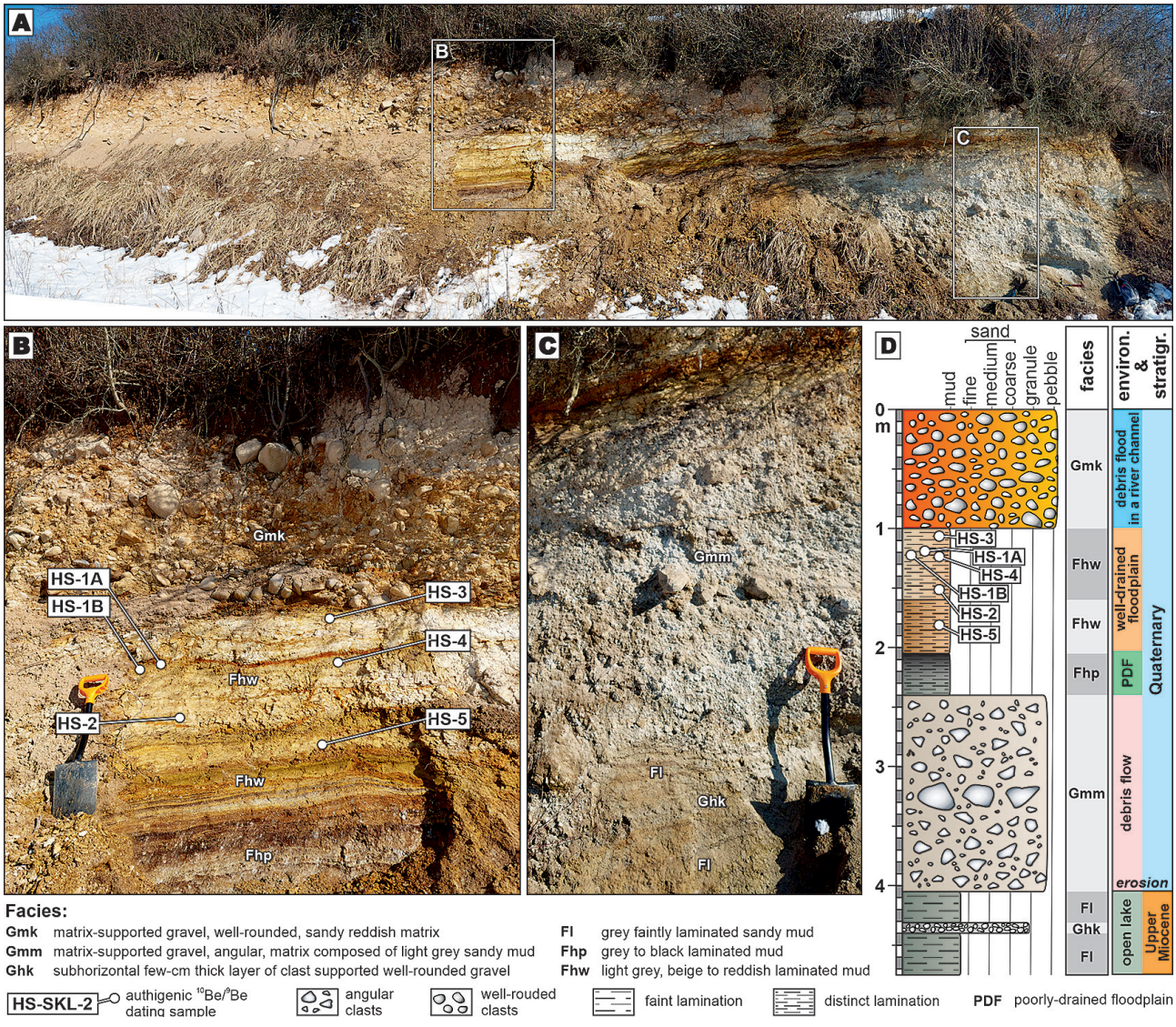

Fig. 4. Horná Štubňa river terrace outcrop. (A) Panoramic view on the outcrop wall, (B, C) details of the facies and sampling points. (D) Synthetic sedimentological log of the outcrop with authigenic 10Be/9Be dating sample positions. See text for explanation of the sedimentary environment and stratigraphic interpretations. Location in Fig. 1D and 2.

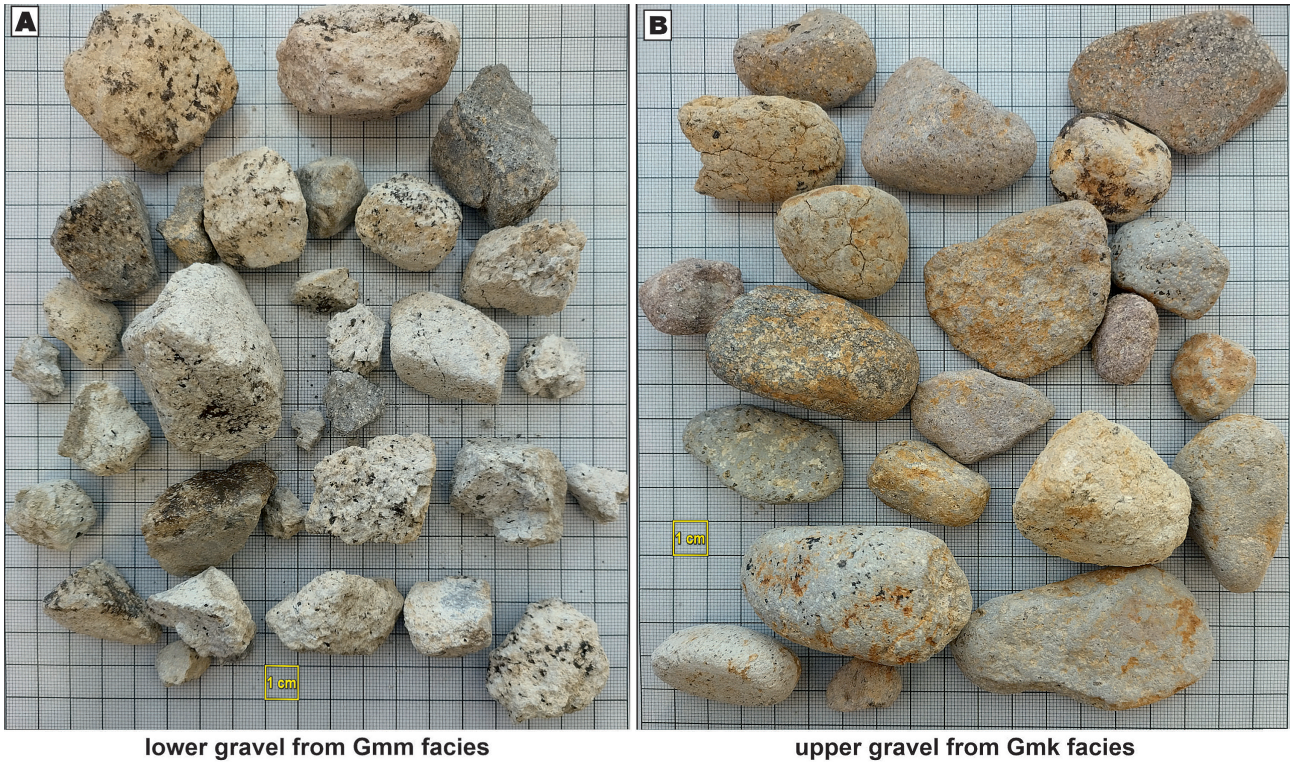

Fig. 5. Examples of gravel from Horná Štubňa river terrace outcrop. (A) Mostly angular, less sub-angular pebbles from the lower gravel level (Gmm facies), interpreted as a subaerial debris flow. (B) Dominantly rounded to well-rounded pebbles from the upper gravel level (Gmk facies), interpreted as a deposit of traction current in a river channel. Note the petrographic similarity of both samples, being composed of andesites and rhyolites. See Fig. 4 for the position of the respective gravel strata.

a continuous channelized stream, given the absence of imbrication, stratification, or any other form of internal organization. Nevertheless, the well-rounded clast nature and sandy matrix imply a fluvial origin of the sediment, likely accumulated near a river channel during periods of increased overflow (Pierson, 2005; Brenna et al., 2020).

4.3. Authigenic ^{10}Be/^{9}Be dating

The measured concentrations of ^{9}Be and ^{10}Be were used to calculate the natural 10Be/9Be ratios of the samples (Tab. 1). These ratios range from 0.998 ± 0.025 (× 10^{-11}) to 1.518 ± 0.039 (× 10^{-11}). The highest ratio, observed in sample HS-3 with a value of 1.518 ± 0.039 (× 10^{-11}), exceeds the initial ratio of Veľký Čepčín, indicating that age calculation is not feasible in this case. The subsequent five samples yielded authigenic ^{10}Be/^{9}Be ages ranging from 394.8 ± 13.2 ka to 724.6 ± 23.6 ka (Tab. 1). The uncertainties do not overlap, and the ages exhibit a scattered pattern (Fig. 6A). However, this age calculation assumes that the Veľký Čepčín site is of sub-recent age, which is not the case (Holec & Braucher, 2014). Consequently, the ages were adjusted by adding the median age of the Veľký Čepčín site (295 ka) and incorporating its age range into the age uncertainties (75 ka), as illustrated in Fig. 6B. The corrected age range of the five samples extends from 689.8 ± 88.2 ka to 1019.6 ± 98.6 ka. Furthermore, the correction resulted in much broader uncertainties, which

Table 1: Concentrations of ^{9}Be and ^{10}Be, ^{10}Be/^{9}Be ratios and calculated ages for the analyzed samples. Uncertainties are 1σ. Concentrations of ^{10}Be are corrected for the AMS ^{10}Be/^{9}Be ratio of two processing blanks with the values of 3.64 × 10^{-14} and 6.17 × 10^{-14}. Despite the relatively high blank isotopic ratios, they are two orders of magnitude higher than the AMS ratios of the dating samples. "V. Čepčín age correction was obtained by adding 295 ka (Veľký Čepčín site age according to Holec & Braucher, 2014) to the radiometric age calculated using Veľký Čepčín initial ratio, and by adding 75 ka to the dating uncertainty.

ID	^{9}Be (at × g^{-1}) × 10^{16}	AMS ^{10}Be/^{9}Be (× 10^{-14})	^{10}Be (at × g^{-1}) × 10^{6}	Natural ^{10}Be/^{9}Be (× 10^{-11})	Age (ka)	
					Veľký Čepčín N_0	V. Čepčín age correction
HS-1A	15.466 ± 0.309	5.392 ± 0.081	1.641 ± 0.025	1.061 ± 0.027	603.0 ± 19.7	898.0 ± 94.7
HS-1B	15.272 ± 0.305	5.071 ± 0.077	1.525 ± 0.023	0.998 ± 0.025	724.6 ± 23.6	1019.6 ± 98.6
HS-2	8.408 ± 0.168	3.164 ± 0.061	0.949 ± 0.018	1.129 ± 0.031	479.1 ± 16.6	774.1 ± 91.6
HS-3	9.151 ± 0.183	4.645 ± 0.077	1.389 ± 0.023	1.518 ± 0.039	n.a. ± n.a.	180.9 ± 71.2
HS-4	13.780 ± 0.276	5.362 ± 0.091	1.622 ± 0.028	1.177 ± 0.031	394.8 ± 13.2	689.8 ± 88.2
HS-5	10.974 ± 0.219	3.972 ± 0.063	1.193 ± 0.019	1.087 ± 0.028	554.2 ± 18.3	849.2 ± 93.3

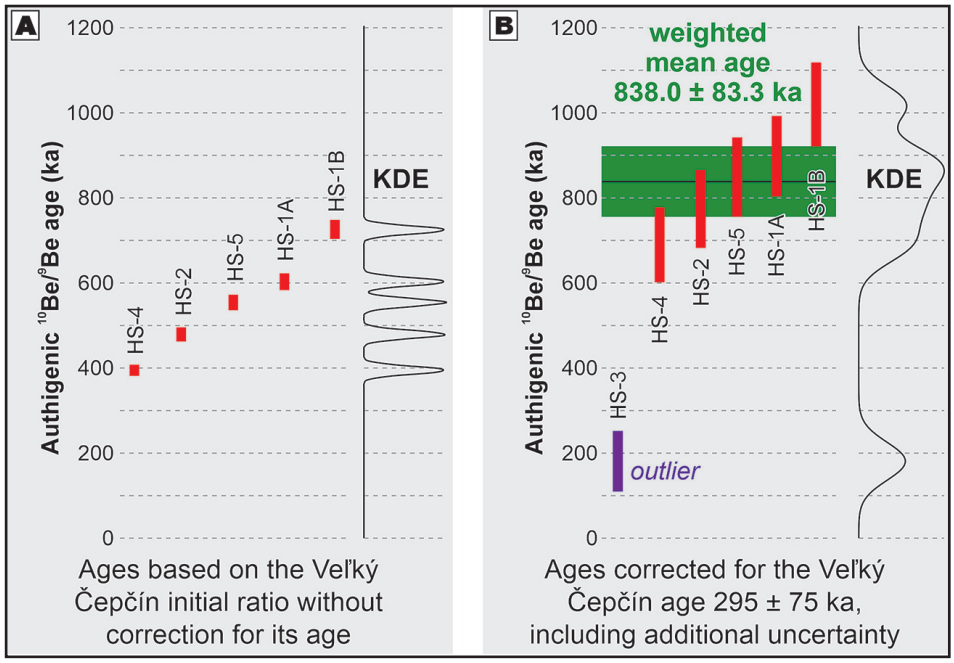

Fig. 6. Authigenic ^{10}Be/^{9}Be ages in ascending order with Kernel density estimation (KDE) obtained using the KDX software (Spencer et al., 2017). (A) represents ages without including the age of the initial ratio calibration site (Veľký Čepčín) into assumption, while (B) shows the same ages corrected for the Veľký Čepčín age and its uncertainty.

overlap within a single population, facilitating the calculation of the weighted mean age of 838.0 ± 83.3 ka (see Fig. 6B).

4.4. Elemental concentrations in the authigenic phase

The concentrations of Al, Fe, and Mn in the authigenic phase of the dating samples are presented in Tab. 2. These values were plotted against the authigenic ^{10}Be/^{9}Be ratios and total ^{9}Be concentrations to investigate potential indications of post-depositional processes, which could contribute to the relatively high scatter of the authigenic ^{10}Be/^{9}Be ages. However, the obtained values revealed no correlations or discernible patterns, except for the Mn concentration, which is notably lower for HS-3 sample compared to the rest of the dataset (Fig. 7).

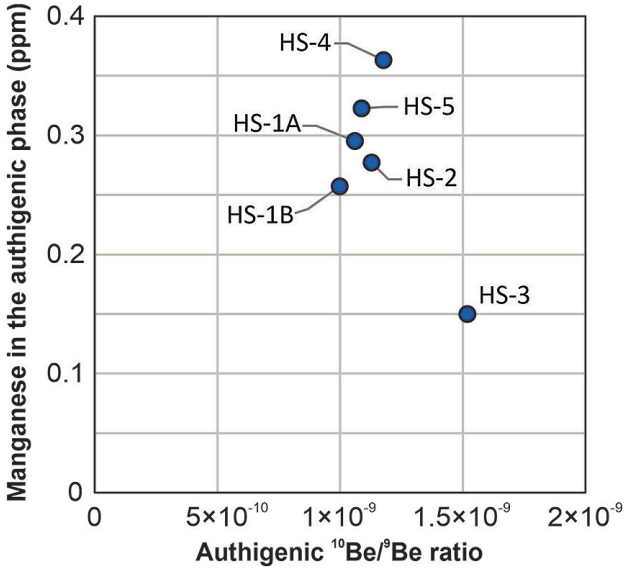

Fig. 7. Authigenic manganese concentrations of the dating samples plotted against the authigenic ^{10}Be/^{9}Be ratios.

Tab. 2: Elemental concentrations in the authigenic phase measured using ICP-MS.

ID	Al	Fe	Mn
	(ppm)	(ppm)	(ppm)
HS-1A	4.89	12.77	0.30
HS-1B	4.25	13.46	0.26
HS-2	6.85	12.99	0.28
HS-3	4.36	22.01	0.15
HS-4	4.96	37.12	0.36
HS-5	7.08	19.33	0.32

5. DISCUSSION AND CONCLUSIONS

5.1. Authigenic ^{10}Be/^{9}Be geochronology

The significant scatter observed in the authigenic ^{10}Be/^{9}Be ages before correcting for the age of the Veľký Čepčín site (refer to Fig. 6A) is likely attributed to the low-accommodation rate depositional conditions typically associated with the formation of river terrace staircases. It has been demonstrated by Šujan et al. (2023c) that base-level fall and subsequent river incision into underlying deposits lead to the redeposition of older mud layers, resulting in an apparent increase in age and greater variability in the obtained ages. Given that the studied site is situated in an intramontane basin characterized by substantial elevation differences and an incised river network, such processes are highly plausible.

The outlier HS-3 sample, exhibiting a ^{10}Be/^{9}Be ratio higher than the initial ratio, was extracted directly from below the base of the gravelly Gmk unit, located in the uppermost part of the floodplain horizon. Its notably different Mn concentration may indicate post-depositional alteration of the authigenic phase, suggesting that the hydrological isolation of the uppermost floodplain layer was not effective. Hence, the stratigraphic position

and composition of the sample support its exclusion from dating assumptions.

The correction applied to the dating results for the Veľký Čepčín site age resulted in significantly wider error bars for individual ages, causing them to overlap. It is noteworthy that the sedimentary environment of the strata subject to dating likely introduces greater variability in the initial 10Be/9Be ratio, in comparison to the analytical uncertainties included in the current calculation approach. This variability could be linked to fluctuations in sediment burial rates, the intensity of pedogenic processes, and the aforementioned redeposition of older mud layers (Šujan et al., 2023a,b). The performed age correction therefore partially supplements the definition of this variability, which should be considered in future research endeavors.

5.2 Depositional evolution

The analyzed succession was deposited during the early stage of the ongoing incision phase of the river network. This is indicated by the spatial position of the accumulation near the basin margins and its relative vertical position in the system, preserving just one higher level (Fig. 3). The lower gravelly unit of the terrace, deposited by debris flow, was supplied by angular colluvial material without being rounded in a river channel, also indicating an early stage of base level fall. The subsequent floodplain deposition records a base level rise and a relative increase in accommodation rate (Martinsen et al., 1999; Püspöki et al., 2013). The muddy nature of this horizon may suggest increased chemical weathering during an interglacial period. The upper gravelly unit with rounded pebbles was deposited on an already well-established river floodplain near a river channel network, from which the pebbles were redeposited during increased overflow, causing debris floods. Both gravelly units bear the same petrography of andesites and rhyolites, highlighting the same source but different transport mechanisms. These rock types are abundant on the margins of the southern Turiec Basin (Fig. 1D).

The corrected weighted mean age of 838.0 ± 3.3 ka for the Horná Štubňa terrace should be approached with caution, as the full extent of uncertainty related to authigenic ^{10}Be/^{9}Be dating of fluvial sediment affected by redeposition of mud in an incising stream is not yet fully understood (Šujan et al., 2023c). Nonetheless, it does offer insights for further consideration. This age suggests the end of the Middle Pleistocene transition (Pisias & Moore, 1981; Clark et al., 2006) as the period when the currently ongoing phase of river incision, associated with river terrace formation, began in the Turiec Basin. Therefore, the presented data may point to the change in climate during the Middle Pleistocene transition as a factor influencing observed changes in the base level of the Turiec Basin.

The resulting incision rate is based on the weighted mean age of 838.0 ± 83.3 ka and the base-level fall of 26–30 m ranges in ~ 0.03–0.04 mm·a^{-1}. This pace of incision is an order of magnitude lower in comparison to the values observed in the Outer Western Carpathians (Olszak & Adamiec, 2016; Olszak, 2017; Olszak et al., 2019; Olszak & Alexanderson, 2020), but fits the ranges documented in the Pannonian Basin and Transdanubian Range areas (Häuselmann et al., 2020; Ruszkiczay-Rüdiger et al., 2020; Šujan et al., 2023c), and also does not deviate much from the low incision rates documented in the Eastern Alps (Wagner et al., 2010, 2011; Legrain et al., 2014; Häuselmann et al., 2020). Future research of river terrace depositional archives will shed more light on the striking difference in incision rates between internal and external zones of the mountain range.

Acknowledgement: The study was supported by the Slovak Research and Development Agency (APVV) under contracts Nos. APVV-16-0121, APVV-20-0120 and APVV-21-0281, and by the Scientific Grant Agency of the Ministry of Education, Science, Research and Sport of the Slovak Republic and the Slovak Academy of Sciences (VEGA) under the contract No. 1/0346/20. The free availability of the Lidar DEM data owned by the Geodesy, Cartography and Cadaster Authority of the Slovak Republic (ÚGKK SR) and distributed by the Geodetic and Cartographic Institute, Bratislava (GKÚ) is acknowledged with gratitude. The ASTER AMS national facility (CEREGE, Aix-en-Provence, France) is supported by the INSU/CNRS, the ANR through the "Projects thématiques d'excellence" program for the "Equipements d'excellence" ASTER-CEREGE action, and IRD. We are grateful to Ladislav Vitovič and an anonymous reviewer for their constructive comments, which were helpful in improving the clarity and conceptual correctness of the manuscript. The precise editorial work of Rastislav Vojtko is highly appreciated.

References

Aslan A. & Autin W.J., 1999: Evolution of the Holocene Mississippi River floodplain, Ferriday, Louisiana: Insights on the origin of fine-grained floodplains. Journal of Sedimentary Research, 69, 4, 800–815.

Blikra L.H. & Nemec W., 1998: Postglacial colluvium in western Norway: depositional processes, facies and palaeoclimatic record. Sedimentology, 45, 5, 909–959.

Bourlès D., Raisbeck G.M. & Yiou F., 1989b: ^{10}Be and ^{9}Be in marine sediments and their potential for dating. Geochimica et Cosmochimica Acta, 53, 2, 443–452.

Braucher R., Guillou V., Bourlès D.L., Arnold M., Aumaître G., Keddadouche K. & Nottoli E., 2015: Preparation of ASTER in-house ^{10}Be/^{9}Be standard solutions. Nuclear Instruments and Methods in Physics Research Section B: Beam Interactions with Materials and Atoms, 361, 335–340.

Braumann S.M., Neuhuber S., Fiebig M., Schaefer J.M., Hintersberger E. & Lüthgens C., 2019: Challenges in constraining ages of fluvial terraces in the Vienna Basin (Austria) using combined isochron burial and pIRIR225 luminescence dating. Quaternary International, 509, 87–102.

Brenna A., Surian N., Ghinassi M. & Marchi L., 2020: Sediment–water flows in mountain streams: Recognition and classification based on field evidence. Geomorphology, 371, 107413.

Brown E.T., Measures C.I., Edmond J.M., Bourlès D.L., Raisbeck G.M. & Yiou F., 1992: Continental inputs of beryllium to the oceans. Earth and Planetary Science Letters, 114, 1, 101–111.

Campo B., Amorosi A. & Bruno L., 2016: Contrasting alluvial architecture of Late Pleistocene and Holocene deposits along a 120-km transect from the central Po Plain (northern Italy). Sedimentary Geology, 341, 265–275.

Chmeleff J., von Blanckenburg F., Kossert K. & Jakob D., 2010: Determination of the ^{10}Be half-life by multicollector ICP-MS and liquid scintillation counting. Nuclear Instruments and Methods in Physics Research Section B: Beam Interactions with Materials and Atoms, 268, 2, 192–199.

Clark P.U., Archer D., Pollard D., Blum J.D., Rial J.A., Brovkin V., Mix A.C., Pisias N.G. & Roy M., 2006: The middle Pleistocene transition: characteristics, mechanisms, and implications for long-term changes in atmospheric pCO2. Quaternary Science Reviews, 25, 23, 3150–3184.

Davies-Vollum K.S. & Kraus M.J., 2001: A relationship between alluvial backswamps and avulsion cycles: an example from the Willwood Formation of the Bighorn Basin, Wyoming. Sedimentary Geology, 140, 3, 235–249.

Deng K., Rickli J., Suhrhoff T.J., Du J., Scholz F., Severmann S., Yang S., McManus J. & Vance D., 2023: Dominance of benthic fluxes in the oceanic beryllium budget and implications for paleo-denudation records. Science Advances, 9, 23, eadg3702.

Dixon J.L., Chadwick O.A. & Pavich M.J., 2018: Climatically controlled delivery and retention of meteoric ^{10}Be in soils. Geology, 46, 10, 899–902.

Dunai T., 2010: Cosmogenic Nuclides. Principles, Concepts and Applications in the Earth Surface Sciences. Cambridge University Press, 187 pp.

Gašparik J., 1972: Záverečná správa o vyhodnotení štruktúrneho vrtu GHŠ-1 Horná Štubňa. Manuscript, Geofond Nr: 31218, 57 pp. Available online: https://da.geology.sk/navigator/?desktop=Public.

Gašparik J. & Halouzka R., 1993: Geologická mapa Turčianskej kotliny, M – 1 : 50 000 (Geological map of the Turiec Basin). State Geological Survey of Dionýz Štúr, Bratislava.

Gibbard P.L. & Lewin J., 2009: River incision and terrace formation in the Late Cenozoic of Europe. Tectonophysics, 474, 1, 41–55.

Häuselmann P., Plan L., Pointner P. & Fiebig M., 2020: Cosmogenic nuclide dating of cave sediments in the eastern alps and implications for erosion rates. International Journal of Speleology, 49, 2, 107-118.

Hók J., Kováč M., Rakús M., Kováč P., Nagy A., Kováčová M., Sitár V. & Šujan M., 1998: Geologic and tectonic evolution of the Turiec depression in the Neogene. Slovak Geological Magazine, 4, 3, 165–176.

Hók J., Šujan M. & Šipka F., 2014: Tectonic division of the Western Carpathians: An overview and a new approach. Acta Geologica Slovaca, 6, 2, 135–143.

Holec J. & Braucher R., 2014: Cosmogenic chlorine dating of alluvial fan (Veľký Čepčín, Turčianska kotlina basin). In: J. Novotný (Ed.), Geomorfológia a environmentálne výzvy. Zborník abstraktov Bratislava, SAV, 2014, pp. 20.

Jelby M.E., Grundvåg S.A., Helland-Hansen W., Olaussen S. & Stemmerik L., 2020: Tempestite facies variability and storm-depositional processes across a wide ramp: Towards a polygenetic model for hummocky cross-stratification. Sedimentology, 67, 2, 742–781.

Konečný V., Lexa J. & Hojstričová V., 1995: The Central Slovakia Neogene volcanic field: a review. Acta Volcanologica, 7, 63–78.

Korschinek G., Bergmaier A., Faestermann T., Gerstmann U., Knie K., Rugel G., Wallner A., Dillmann I., Dollinger G. & Von Gostomski C.L., 2010: A new value for the half-life of ^{10}Be by heavy-ion elastic recoil detection and liquid scintillation counting. Nuclear Instruments and Methods in Physics Research Section B: Beam Interactions with Materials and Atoms, 268, 2, 187–191.

Kováč M., Hók J., Minár J., Vojtko R., Bielik M., Pipík R., Rakús M., Kráľ J., Šujan M. & Králiková S., 2011: Neogene and Quaternary development of the Turiec Basin and landscape in its catchment: A tentative mass balance model. Geologica Carpathica, 62, 4, 361–379.

Kováč M., Plašienka D., Soták J., Vojtko R., Oszczypko N., Less G., Ćosović V., Fügenschuh B. & Králiková S., 2016: Paleogene palaeogeography and basin evolution of the Western Carpathians, Northern Pannonian domain and adjoining areas. Global and Planetary Change, 140, 9–27.

Kováč P. & Hók J., 1993: The Central Slovak Fault System - the field evidence of a strike slip. Geologica Carpathica, 44, 3, 155–159.

Králiková S., Vojtko R., Andriessen P., Kováč M., Fuegenschuh B., Hók J. & Minár J., 2014: Late Cretaceous-Cenozoic thermal evolution of the northern part of the Central Western Carpathians (Slovakia): revealed by zircon and apatite fission track thermochronology. Tectonophysics, 615, 142–153.

Lebatard A.E., Bourlès D.L., Duringer P., Jolivet M., Braucher R., Carcaillet J., Schuster M., Arnaud N., Monié P., Lihoreau F., Likius A., Mackaye H.T., Vignaud P. & Brunet M., 2008: Cosmogenic nuclide dating of Sahelanthropus tchadensis and Australopithecus bahrelghazali: Mio-Pliocene hominids from Chad. Proceedings of the National Academy of Sciences of the United States of America, 105, 9, 3226–3231.

Legrain N., Stüwe K. & Wölfler A., 2014: Incised relict landscapes in the eastern Alps. Geomorphology, 221, 124-138.

Lexa J., Seghedi I., Nemeth K., Szakacs A., Konecny V., Pecskay Z., Fueloep A. & Kovacs M., 2010: Neogene-Quaternary Volcanic forms in the Carpathian–Pannonian Region: a review. Central European Journal of Geosciences, 2, 3, 207–U75.

Martinsen O.J., Ryseth A., Helland-Hansen W., Flesche H., Torkildsen G. & Idil S., 1999: Stratigraphic base level and fluvial architecture: Ericson Sandstone (Campanian), Rock Springs Uplift, SW Wyoming, USA. Sedimentology, 46, 2, 235–259.

Measures C. & Edmond J., 1983: The geochemical cycle of 9Be: A reconnaissance. Earth and Planetary Science Letters, 66, 101–110.

Merchel S. & Herpers U., 1999: An update on radiochemical separation techniques for the determination of long-lived radionuclides via accelerator mass spectrometry. Radiochimica acta, 84, 4, 215–220.

Minár J., Bielik M., Kováč M., Plašienka D., Barka I., Stankoviansky M. & Zeyen H., 2011: New morphostructural subdivision of the Western Carpathians: An approach integrating geodynamics into targeted morphometric analysis. Tectonophysics, 502, 1–2, 158–174.

Mulder T., Syvitski J.P.M., Migeon S., Faugeres J.C. & Savoye B., 2003: Marine hyperpycnal flows: initiation, behavior and related deposits. A review. Marine and Petroleum Geology, 20, 6–8, 861–882.

Necea D., Fielitz W. & Matenco L., 2005: Late Pliocene-Quaternary tectonics in the frontal part of the SE Carpathians: Insights from tectonic geomorphology. Tectonophysics, 410, 1–4, 137–156.

Necea D., Fielitz W., Kadereit A., Andriessen P.A.M. & Dinu C., 2013: Middle Pleistocene to Holocene fluvial terrace development and uplift-driven valley incision in the SE Carpathians, Romania. Tectonophysics, 602, 332–354.

Nemčok M. & Lexa J., 1990: Evolution of the basin and range structure around the Žiar mountain range. Geologica Carpathica, 41, 229–258.

Novák A., Bábek O. & Kapusta J., 2017: Late Quaternary tectonic switching of siliciclastic provenance in the strike-slip-dominated foreland of the Western Carpathians; Upper Morava Basin, Bohemian Massif. Sedimentary Geology, 355, 58–74.

Olszak J., 2017: Climatically controlled terrace staircases in uplifting mountainous areas. Global and Planetary Change, 156, 13–23.

Olszak J. & Adamiec G., 2016: OSL-based chronostratigraphy of river terraces in mountainous areas, Dunajec basin, West Carpathians: a revision of the climatostratigraphical approach. Boreas, 45, 3, 483–493.

Olszak J. & Alexanderson H., 2020: Post-IR IRSL dating the oldest (?) river terrace sediments in the Polish Outer Carpathians: Insights into the landscape evolution. Geomorphology, 371, 107436

Olszak J., Kukulak J. & Alexanderson H., 2019: Climate control on alluvial sediment storage in the northern foreland of the Tatra Mountains since the late Pleistocene. Quaternary Research (United States), 91, 2, 848–860.

Pierson T.C., 2005: Distinguishing between debris flows and floods from field evidence in small watersheds. 2327–6932, US Geological Survey.

Pierson T.C. & Costa J.E., 1987: A rheologic classification of subaerial sediment-water flows. In: Costa J.E. & Wieczorek G.F. (Eds.), Debris Flows/Avalanches: Process, Recognition, and Mitigation. Reviews in Engineering Geology. Geological Society of America, pp. 1–12.

Pipík R., Bodergat A.M., Briot D., Kováč M., Král J. & Zielinski G., 2012: Physical and biological properties of the late Miocene, long-lived Turiec Basin, Western Carpathians (Slovakia) and its paleobiotopes. Journal of Paleolimnology, 47, 2, 233–249.

Pisias N.G. & Moore T.C., 1981: The evolution of Pleistocene climate: A time series approach. Earth and Planetary Science Letters, 52, 2, 450–458.

Plašienka D., 2018: Continuity and Episodicity in the Early Alpine Tectonic Evolution of the Western Carpathians: How Large-Scale Processes Are Expressed by the Orogenic Architecture and Rock Record Data. Tectonics, 37, 7, 2029–2079.

Plink-Björklund P., 2021: Distributive Fluvial Systems: Fluvial and Alluvial Fans. In: Alderton D. & Elias S.A. (Eds.), Encyclopedia of Geology (Second Edition). Academic Press, Oxford, pp. 745–758.

Püspöki Z., Demeter G., Tóth-Makk Á., Kozák M., Dávid Á., Virág M., Kovács-Pálffy P., Kónya P., Gyuricza G., Kiss J., McIntosh R.W., Forgács Z., Buday T., Kovács Z., Gombos T. & Kummer I., 2013: Tectonically controlled Quaternary intracontinental fluvial sequence development in the Nyírség–Pannonian Basin, Hungary. Sedimentary Geology, 283, 0, 34–56.

Raisbeck G.M., Yiou F., Fruneau M., Loiseaux J.M., Lievin M. & Ravel J.C., 1981: Cosmogenic ^{10}Be/^{7}Be as a probe of atmospheric transport processes. Geophysical Research Letters, 8, 9, 1015–1018.

Ruszkiczay-Rüdiger Z., Balázs A., Csillag G., Drijkoningen G. & Fodor L., 2020: Uplift of the Transdanubian Range, Pannonian Basin: How fast and why? Global and Planetary Change, 192, 103263.

Ruszkiczay-Rüdiger Z., Csillag G., Fodor L., Braucher R., Novothny Á., Thamó-Bozsó E., Virág A., Pazonyi P. & Timár G., 2018: Integration of new and revised chronological data to constrain the terrace evolution of the Danube River (Gerecse Hills, Pannonian Basin). Quaternary Geochronology, 48, 148–170.

Schumacher M., Dobos A., Schier W. & Schütt B., 2018: Holocene valley incision in the southern Bükk foreland: Climate-human-environment interferences in northern Hungary. Quaternary International, 463, 91–109.

Singleton A.A., Schmidt A.H., Bierman P.R., Rood D.H., Neilson T.B., Greene E.S., Bower J.A. & Perdrial N., 2017: Effects of grain size, mineralogy, and acid-extractable grain coatings on the distribution of the fallout radionuclides ^{7}Be, ^{10}Be, 137_{Cs}, and 210_{Pb} in river sediment. Geochimica et Cosmochimica Acta, 197, 71–86.

Sládek J., Vitovič L., Holec J. & Hók J., 2022: Results of the Morphotectonics and Fluvial Activity of Intramountain Basins: The Turčianska Kotlina and Žiarska Kotlina Basins. In: Lehotský M. & Boltižiar M. (Eds.), Landscapes and Landforms of Slovakia. World Geomorphological Landscapes, pp. 207–233.

Spencer C.J., Yakymchuk C. & Ghaznavi M., 2017: Visualising data distributions with kernel density estimation and reduced chi-squared statistic. Geoscience Frontiers, 8, 6, 1247–1252.

Starkel L., Gelbica P. & Superson J., 2007: Last Glacial–Interglacial cycle in the evolution of river valleys in southern and central Poland. Quaternary Science Reviews, 26, 22, 2924–2936.

Stow D.A., 2005: Sedimentary Rocks in the Field. A Colour Guide. Manson Publishing, London, 320 pp.

Šujan M. & Dzúrik J., 1996: Horná Štubňa - združená skládka odpadov - monitorovací systém, podrobný prieskum geologických činiteľov životného prostredia. Equis. Bratislava, 18 pp. Manuscript, Geofond Nr. 80887, available online at: https://da.geology.sk/navigator/?desktop=Public.

Šujan M. & Rybár S., 2014: The development of Pleistocene river terraces in the eastern part of the Danube Basin. Acta Geologica Slovaca, 6, 2, 107–122 [in Slovak with English summary].

Šujan M., Braucher R., Kováč M., Bourlès D.L., Rybár S., Guillou V. & Hudáčková N., 2016: Application of the authigenic ^{10}Be/^{9}Be dating method to Late Miocene–Pliocene sequences in the northern Danube Basin (Pannonian Basin System): Confirmation of heterochronous evolution of sedimentary environments. Global and Planetary Change, 137, 35–53.

Šujan M., Aherwar K., Chyba A., Rózsová B., Braucher R., Šujan M., Šipka F. & AsterTeam, 2023a: Sedimentological and geochronological data for the fan deltaic Nemčiňany Formation, Upper Miocene, Danube Basin (Slovakia). Mendeley Data, https://doi.org/10.31577/GeolCarp.2023.25.

Šujan M., Aherwar K., Vojtko R., Braucher R., Šarinová K., Chyba A., Hók J., Grizelj A., Pipík R., Lalinská-Voleková B., Rózsová B. & Team A., 2023b: Application of the authigenic ^{10}Be/^{9}Be dating to constrain the age of a long-lived lake and its regression in an isolated intermontane basin: The case of Late Miocene Lake Turiec, Western Carpathians. Palaeogeography, Palaeoclimatology, Palaeoecology, 628, 111746.

Šujan M., Braucher R., Chyba A., Vlačiky M., Aherwar K., Rózsová B., Fordinál K., Maglay J., Nagy A., Moravcová M. & AsterTeam, 2023c: Mud redeposition during river incision as a factor affecting authigenic ^{10}Be/^{9}Be dating: Early Pleistocene large mammal fossil-bearing site Nová Vieska, eastern Danube Basin. Journal of Quaternary Science, 38, 3, 347–364.

Šujan M., Aherwar K., Vojtko R., Braucher R., Šarinová K., Chyba A., Hók J., Grizelj A., Pipík R., Lalinská-Voleková B., Rózsová B. & Team A., 2024: Stratigraphic, sedimentological, geochemical, mineralogical and geochronological data characterizing the Upper Miocene sequence of the Turiec Basin, Western Carpathians (Central Europe). Data in Brief, 52, 109810.

Šustek M., 2001: I/65 Horná Štubňa – obchvat, orientačný IGP a doplnenie orientačného prieskumu. Šustek – I.G. Prieskum, Žilina, 17 pp. Manuscript, Geofond Nr. 83613, available online at: https://da.geology.sk/navigator/?desktop=Public.

Talling P.J., Masson D.G., Sumner E.J. & Malgesini G., 2012: Subaqueous sediment density flows: Depositional processes and deposit types. Sedimentology, 59, 7, 1937–2003.

Tan S.H. & Horlick G., 1987: Matrix-effect observations in inductively coupled plasma mass spectrometry. Journal of Analytical Atomic Spectrometry, 2, 8, 745–763.

Tlapáková L., Pánek T. & Horáčková Š., 2021: Holocene fluvial terraces reveal landscape changes in the headwater streams of the Moravskoslezské Beskydy Mountains, Czechia. Geomorphology, 377, 107589.

Tužinský A., Banský V. & Potyš Z., 1967: Povodie Turca - orientačný HGP riečnych náplavov. IGHP, Žilina, 117 pp. Manuscript, Geofond Nr. 18205, available online at: https://da.geology.sk/navigator/?desktop=Public.

Vandenberghe J., 2008: The fluvial cycle at cold–warm–cold transitions in lowland regions: A refinement of theory. Geomorphology, 98, 3, 275–284.

Viveen W., Braucher R., Bourlès D., Schoorl J.M., Veldkamp A., van Balen R.T., Wallinga J., Fernandez-Mosquera D., Vidal-Romani J.R. & Sanjurjo-Sanchez J., 2012: A 0.65 Ma chronology and incision rate assessment of the NW Iberian Miño River terraces based on ^{10}Be and luminescence dating. Global and Planetary Change, 94–95, 82–100.

Vitovič L. & Minár J., 2018: Morphotectonic analysis for improvement of neotectonic subdivision of the Liptovská Kotlina Basin (Western Carpathians). Geografický Časopis, 70, 3, 197–216.

Vojtko R., Marko F., Preusser F., Madarás J. & Kováčová M., 2011: Late quaternary fault activity in the western Carpathians: Evidence from the vikartovce fault (Slovakia). Geologica Carpathica, 62, 6, 563–574.

Wagner T., Fabel D., Fiebig M., Häuselmann P., Sahy D., Xu S. & Stüwe K., 2010: Young uplift in the non-glaciated parts of the Eastern Alps. Earth and Planetary Science Letters, 295, 1–2, 159–169.

Wagner T., Fritz H., Stüwe K., Nestroy O., Rodnight H., Hellstrom J. & Benischke R., 2011: Correlations of cave levels, stream terraces and planation surfaces along the River Mur–Timing of landscape evolution along the eastern margin of the Alps. Geomorphology, 134, 1–2, 62–78.

Willenbring J.K. & von Blanckenburg F., 2010: Meteoric cosmogenic Beryllium-10 adsorbed to river sediment and soil: Applications for Earth-surface dynamics. Earth-Science Reviews, 98, 1–2, 105–122.

Wittmann H., von Blanckenburg F., Bouchez J., Dannhaus N., Naumann R., Christl M. & Gaillardet J., 2012: The dependence of meteoric ^{10}Be concentrations on particle size in Amazon River bed sediment and the extraction of reactive ^{10}Be/^{9}Be ratios. Chemical Geology, 318, 126–138.

Yawar Z. & Schieber J., 2017: On the origin of silt laminae in laminated shales. Sedimentary Geology, 360, 22–34.